Available online at www.sciencedirect.com
ScienceDirect
Toxicology and Applied Pharmacology 217 (2006) 308–321
Toxicology and Applied Pharmacology
www.elsevier.com/locate/ytaap

Developmental toxicity of 4-ring polycyclic aromatic hydrocarbons in zebrafish is differentially dependent on AH receptor isoforms and hepatic cytochrome P4501A metabolism

John P. Incardona *, Heather L. Day, Tracy K. Collier, Nathaniel L. Scholz

Ecotoxicology and Environmental Fish Health Program, Environmental Conservation Division, Northwest Fisheries Science Center, 2725 Montlake Blvd E, Seattle, WA 98112, USA

Received 18 August 2006; revised 26 September 2006; accepted 26 September 2006
Available online 7 October 2006

Abstract

Polycyclic aromatic hydrocarbons (PAHs) derived from fossil fuels are ubiquitous contaminants and occur in aquatic habitats as highly variable and complex mixtures of compounds containing 2 to 6 rings. For aquatic species, PAHs are generally accepted as acting through either of two modes of action: (1) "dioxin-like" toxicity mediated by activation of the aryl hydrocarbon receptor (AHR), which controls a battery of genes involved in PAH metabolism, such as cytochrome P4501A (CYP1A) and (2) "nonpolar narcosis", in which tissue uptake is dependent solely on hydrophobicity and toxicity is mediated through non-specific partitioning into lipid bilayers. As part of a systematic analysis of mechanisms of PAH developmental toxicity in zebrafish, we show here that three tetracyclic PAHs (pyrene, chrysene, and benz[*a*]anthracene) activate the AHR pathway tissue-specifically to induce distinct patterns of CYP1A expression. Using morpholino knockdown of *ahr1a*, *ahr2*, and *cyp1a*, we show that distinct embryolarval syndromes induced by exposure to two of these compounds are differentially dependent on tissue-specific activation of AHR isoforms or metabolism by CYP1A. Exposure of embryos with and without circulation (*silent heart* morphants) resulted in dramatically different patterns of CYP1A induction, with circulation required to deliver some compounds to internal tissues. Therefore, biological effects of PAHs cannot be predicted simply by quantitative measures of AHR activity or a compound's hydrophobicity. These results indicate that current models of PAH toxicity in fish are greatly oversimplified and that individual PAHs are pharmacologically active compounds with distinct and specific cellular targets.
Published by Elsevier Inc.

Keywords: Fossil fuels; Non-point source pollution; Fish development; Cardiotoxicity; Hepatotoxicity; Mixture toxicity

Introduction

Complex mixtures of PAHs derived from fossil fuels and their combustion are signatures of industrialization and urbanization, and they contribute to both air and water pollution. Despite declines in PAH levels in urban watersheds late in the last century, new increases in aquatic PAH accumulation over the last decade have been detected and are associated with increased use of motor vehicles (Van Metre et al., 2000; Lima et al., 2002; Partridge et al., 2005). Stormwater runoff and atmospheric deposition are now the largest sources of aquatic PAH contamination (Van Metre et al., 2000; Lima et al., 2002; National Research Council, 2003; Van Metre and Mahler, 2003; Li and Daler, 2004), and this is expected to increase with continued coastal development. A full appreciation of the impacts of urbanization and non-point source pollution on key marine and aquatic resources requires a more detailed understanding of mechanisms of PAH toxicity. Such an understanding is crucial because there is scant experimental support for current PAH toxicity models that could be used to establish water or sediment quality guidelines for regulating PAH levels and protecting sensitive aquatic life (Di Toro et al., 2000; French-McCay, 2002; U.S. EPA, 2003; Barron et al., 2004a; Barron et al., 2004b; French-McCay, 2004).

A wide range of studies indicate that fish embryos and larvae are highly sensitive to PAH mixtures from a variety of sources, including crude oil spills, creosote wood preservatives, oil

* Corresponding author. Fax: +1 206 860 3335.
E-mail address: john.incardona@noaa.gov (J.P. Incardona).

0041-008X/$ - see front matter. Published by Elsevier Inc.
doi:10.1016/j.taap.2006.09.018

sands, and sediments impacted by urbanization (Carls et al., 1999; Heintz et al., 1999; Heintz et al., 2000; Vines et al., 2000; Couillard, 2002; Colavecchia et al., 2004; Sundberg et al., 2005). However, the composition of PAH mixtures can vary considerably depending on the relative contributions from petrogenic (e.g. oil spills) or pyrogenic (i.e. combustive) sources. In general, petroleum products are enriched with low molecular weight PAHs containing two or three rings, while fuel combustion products contain a higher percentage and variety of high molecular weight compounds with four rings and greater. There is a long-held view that PAHs containing 2–4 rings, with their simple carbon–hydrogen structure and lack of functional groups, have no specific toxicity and act acutely through general disruption of membranes or "narcosis". This is based on a linear relationship between the lethal concentrations of PAH killing 50% of test organisms (LC_{50}) and hydrophobicity expressed as the log octanol–water partition coefficient (K_{ow}) (Di Toro et al., 2000), similar to classical studies relating anesthetic potency to hydrophobicity. Models describing this relationship assume that organisms take up hydrophobic compounds passively into a single compartment following first order kinetics (Mackay, 1982; Mackay et al., 1992a; McCarty et al., 1992). Similarly, they predict a trade-off between water solubility and K_{ow}, where compounds with log $K_{ow} > 5.6$ would be non-toxic due to insufficient bioavailability (French-McCay, 2002).

On the other hand, the high molecular weight PAHs include many compounds that are relatively strong agonists of the AHR, while low molecular weight PAHs are poor AHR agonists. The AHR is a ligand-activated basic-helix-loop-helix-Per-Arnt-Sim (bHLH-PAS) family transcription factor that controls the expression of a battery of genes encoding enzymes that convert PAHs to water-soluble derivates that are excreted, including mixed function oxygenases such as CYP1A family members (Schmidt and Bradfield, 1996; Nebert et al., 2004). Due to the production of reactive intermediates by CYP1A, many high molecular weight PAHs are carcinogenic, and it is widely held that PAH toxicity is mediated through this metabolic pathway. However, the contributions of AHR activation to the developmental toxicity of complex PAH mixtures are not clearly defined. To gain insight into the effects of complex PAH mixtures on fish early life history stages, we are carrying out a systematic analysis of the developmental toxicity of individual PAH compounds in zebrafish (*Danio rerio*).

As a consequence of the Exxon Valdez oil spill, weathered Alaska North Slope (ANS) crude oil is one of the most intensively studied complex PAH mixtures. Exposure of fish embryos to weathered ANS oil and similar PAH mixtures causes a syndrome of pericardial and yolk sac edema, reduced craniofacial structures, and body axis defects (Marty et al., 1997; Carls et al., 1999; Heintz et al., 1999; Couillard, 2002; Pollino and Holdway, 2002; Incardona et al., 2005). Many of these defects are induced by exposure to the individual tricyclic AHs representing the most abundant classes in weathered ANS oil and are secondary to impacts on embryonic cardiac function that are coincident with development of the cardiac conduction system (Incardona et al., 2004; Incardona et al., 2005; Milan et al., 2006). Phenanthrenes, fluorenes and dibenzothiophenes cause embryonic cardiac dysfunction in an AHR- and CYP1A-independent manner, probably by targeting cardiac ion channels (Incardona et al., 2004; Incardona et al., 2005).

Exposure of fish embryos to highly potent AHR ligands such as 2,3,7,8-tetrachlorodibenzo-*p*-dioxin (TCDD) induces a superficially similar syndrome marked by pericardial and yolk sac edema, vascular dysfunction, and defects in heart development (Peterson et al., 1993). However, dioxins are distinct from PAHs in that they are not metabolized by CYP1A and therefore have the ability to bioaccumulate and persistently activate the AHR pathway. In zebrafish, a brief exposure to TCDD shortly after fertilization results in the appearance of the dioxin toxicity syndrome in hatching-stage larvae at 72–96 h post-fertilization (hpf) (Henry et al., 1997; Belair et al., 2001). These effects of TCDD exposure require a functional AHR.

While mammals and birds have a single AHR, fish species possess two AHR clades, AHR1 and AHR2, which were derived from an independent duplication event prior to the wholesale genome duplication that occurred early in the teleost lineage (Hahn, 2002). A variety of analyses indicate that fish AHR1 is orthologous to the single mammalian AHRs, while AHR2 is a divergent paralog. Three AHR genes have been identified in the zebrafish genome, a pair of AHR1 co-orthologs (*ahr1a* and *ahr1b*) and a single *ahr2*. The *ahr1b* and *ahr2* genes exist as a tandem duplication on chromosome 22, while *ahr1a* resides on chromosome 16 (Andreasen et al., 2002; Karchner et al., 2005). Several lines of evidence have suggested that AHR2 is the predominant form in fish (Hahn and Karchner, 1995; Roy and Wirgin, 1997; Abnet et al., 1999a; Karchner et al., 1999; Andreasen et al., 2002). Earlier characterizations of AHR2 and AHR1A in zebrafish demonstrated that only AHR2 had properties that define the mammalian AHR, including high affinity TCDD binding, formation of heterodimers with the AHR nuclear translocator factor, and subsequent xenobiotic response element binding with activation of transcription (Abnet et al., 1999b; Tanguay et al., 1999; Andreasen et al., 2002). More recently, these properties were shown for AHR1B (Karchner et al., 2005). However, the physiological significance of AHR1 isoforms in zebrafish is not yet clear. In the adult, *ahr1a* is expressed predominantly in the liver, while *ahr2* mRNA is more abundant in a variety of other tissues (Andreasen et al., 2002). The tissue distribution of *ahr1b* was not determined, but its total mRNA levels in the embryo were much higher than *ahr1a* (Karchner et al., 2005). Although AHR1B possesses TCDD-inducible transcriptional activity, the developmental toxicity of TCDD in zebrafish appears to require only a functional AHR2: antisense morpholino knockdown of *ahr2* protects embryos from TCDD toxicity (Prasch et al., 2003; Teraoka et al., 2003). However, *cyp1a* knockdown did not influence the effects of dioxin on zebrafish embryos, implicating other AHR target genes in the pathophysiology of dioxin developmental toxicity (Carney et al., 2004).

Here we continue our systematic analysis of PAH toxicity in fish embryos with a comparison of three tetracyclic AHs: pyrene, chrysene, and benz[*a*]anthracene. Because of their relative potency as AHR agonists compared to the tricyclic

AHs, these compounds might be expected to cause AHR-dependent toxicity. Using morpholino knockdown of *ahr1a*, *ahr2*, and *cyp1a*, we show that distinct embryolarval syndromes induced by exposure to pyrene or benz[*a*]anthracene are differentially dependent on tissue-specific activation of AHR isoforms or metabolism by CYP1A. Using genetic ablation of circulatory function in conjunction with the distinct tissue-specific patterns of CYP1A induction associated with each tetracyclic AH, we tested whether PAH uptake is an active or passive process. The results indicate that current models of PAH toxicity in fish are vastly oversimplified and that PAHs should be considered as pharmacologically active compounds with specific cellular targets.

Table 1
PAHs used in the studies

PAH	MW	Water solubility (μM)	Log K_{ow} [a]	AHR fish potency factor [b]
Pyrene	202.2	0.67	5.18	3.85×10^{-7}
Chrysene	228.3	0.0088	5.86	6.59×10^{-5}
Benz[*b*]anthracene	228.3	0.0026	5.76	1.4×10^{-4}
Benz[*a*]anthracene	228.3	0.048	5.91	2×10^{-4}

AHR fish potency factors represent a combination of AHR affinity and potency at CYP1A induction relative to a potency of 1 for TCDD.
[a] Mackay et al., 1992b.
[b] Barron et al., 2004b.

Methods

Chemicals. Pyrene (>99% purity), chrysene (98%), benz[*a*]anthracene (1,2-benzanthracene, 99%), and benz[*b*]anthracene (2,3-benzanthracene, 98%), 2,3-butanedione monoxeme, and MS-222 were obtained from Sigma-Aldrich, St. Louis, MO. Stock PAH solutions were made in dimethyl sulfoxide (DMSO, tissue culture grade, Sigma) at 5–10 mg/ml except benz[*b*]anthracene at 0.5 mg/ml. Final concentrations of DMSO were 0.1% or lower in exposure medium.

Zebrafish exposures. Wild type AB strain zebrafish were maintained and fertilized eggs obtained as previously described (Incardona et al., 2004; Incardona et al., 2005). Fish were treated according to an IACUC-approved protocol and anesthetized with ~1 mM MS-222 when necessary. Exposures to individual model PAH compounds were carried out in plastic 6-well plates (15–25 embryos in 3 ml, 2–3 well replicates) or plastic 150 mm petri dishes (up to 50 embryos in 40 ml) with a static renewal protocol at 28.5 °C as described previously (Incardona et al., 2004; Incardona et al., 2005). All exposures utilized doses above the solubility limit of the compounds. For toxic PAHs, this produced effects in 100% of the embryos. Each experiment was conducted at least three times with similar results. All reported statistical analysis was performed with JMP 5.1.2 for Macintosh (SAS, Cary, NC).

Morpholino injections. Morpholino oligonucleotides (GeneTools, Philomath, OR) included translation-blocking morpholinos targeting zebrafish AHR2 (5′-TGTACCGATACCCGCCGACATGGTT-3′, *ahr2*-MO), CYP1A (5′-TGGATACTTTCCAGTTCTCAGCTCT-3′, *cyp1a*-MO) (Teraoka et al., 2003), and *silent heart*/cardiac troponin T (5′-CATGTTTGCTCTGATCTGA-CACGCA-3′, *sih*-MO) (Sehnert et al., 2002); and a splice-blocking morpholino targeting the AHR1A exon 2/intron 2 splice donor site (5′-CTTTTGAAGT-GACTTTTGGCCCGCA-3′, *ahr1a*-MO) (Incardona et al., 2005). Negative control morpholinos included mismatched oligonucleotides for AHR2 (5′-TGaACCcATACCCGCCGtCATcGTT-3′, 4Mis-*ahr2*-MO) and AHR1A (5′-CTTTTcAAcTGAgTTTTGcCCCcCA-3, 5mis-*ahr1a*-MO), and a generic "standard control" (5′-CCTCTTACCTCAGTTACAATTTATA-3′, std-MO). Embryos were injected at the 1- to 4-cell stage (0.25–1 hpf) with a maximum volume of 4 nl morpholino solution (100 μM) using a PLI90 Picoinjector (Harvard Apparatus, Holliston, MA). Injection volume was calculated after measuring the diameter of a droplet injected into heavy oil. Injected embryos were allowed to recover in system water at 28.5 °C to 50% epiboly (5–6 h) before use in exposure studies. For fluorescein- or rhodamine-conjugated morpholinos (*ahr1a*-MO, 5mis-*ahr1a*-MO, *cyp1a*-MO, and std-MO), embryos were selected on an epifluorescent stereoscope based on fluorescence intensity and an even distribution in blastomeres. No obvious phenotypic changes were produced by *ahr1a*, *ahr2*, or *cyp1a* morpholinos in embryos that were left untreated or exposed to solvent alone, but the morphants were not examined for specific defects.

Reverse transcriptase PCR assays of ahr1a splicing and cyp1a transcript abundance. Total RNA was isolated from 30 to 100 embryos or larvae for each treatment group. Animals were anesthetized and flash frozen on liquid nitrogen prior to storage at −80 °C. Embryos were disrupted using handheld Pellet Pestle Motor and Rnase free pestles and tubes (Kontes Glass Company, Vineland, NJ), homogenized with QIAshredders (QIAGEN, Valencia, CA) and RNA isolated using the RNeasy Protect Mini Kit (QIAGEN) according to the manufacturer's instructions. RNA was quantified on a NanoDrop ND-1000 spectrophotometer (NanoDrop Technologies, Wilmington, DE), and quality verified by an optical density (OD) absorption ratio OD 260 nm/OD 280 nm > 1.9 and agarose electrophoresis of 1 μg RNA. Efficacy of *ahr1a*-MO splice blocking was assessed with reverse transcriptase (RT) PCR. Primers spanning *ahr1a* exon 2 were 5′-CGCAAAAGGAGGAAACCTGTC-3′ (forward) and 5′-CCTGTAG-CAAAAATTCCCCCT-3′ (reverse). Oligonucleotide primers were synthesized by Sigma/Genosys (The Woodlands, TX). Total larval zebrafish RNA was reverse transcribed using SuperScript III First-Strand Synthesis SuperMix and either random hexamer primers for splice site analysis or oligo(dT)20 for Q-PCR assay (Invitrogen, Carlsbad, CA) according to manufacturer's instructions. Template cDNA was amplified by PCR using Platinum Taq DNA polymerase (Invitrogen) under the following conditions for 50 μl reactions: 94 °C for 10 min followed by 35 cycles of 94 °C for 15 s, 56.7 °C for 30 s, 72 °C for 45 s, and one final extension step at 72 °C for 7 min. Cryptic splice variation was analyzed by digesting PCR products at a unique *Hpa*I restriction enzyme site (New England

Fig. 1. Exposure to tetracyclic AHs results in different patterns and degrees of CYP1A induction. Zebrafish embryos were exposed to pyrene (25 μM), chrysene (22 μM), or benz[*a*]anthracene (22 μM) from 6 hpf to 72 hpf, and fixed and processed for CYP1A and myosin heavy chain immunofluorescence (A–I), or frozen for total RNA isolation and quantification of CYP1A mRNA (J). In all images anterior is to the left and dorsal at top; scale bars are 200 μm (A, D, G) and 50 μm (B, C, E, F, H, I). Confocal imaging of CYP1A immunofluorescence is shown in panels A–I, while merged images (C′, F′, I′) show CYP1A immunofluorescence (green) and myocardial myosin heavy chain (red). Panels A–C, pyrene exposure induced CYP1A in the major and minor blood vessels of the head region (A), hepatocytes (B), and the endocardium (C, arrow) but not myocardium (C′, unfilled arrowhead). Panels D–F, chrysene exposure induced CYP1A in the epidermis and head blood vessels (D), but not in hepatocytes (E), and in endocardium (F, arrow) but not myocardium (F′, unfilled arrowhead). Panels G–I, benz[*a*]anthracene exposure induced CYP1A throughout the blood vessels of the head (G), in hepatocytes (H), the endocardium (I, arrow), and myocardium (I′, filled arrowhead). Only very weak background labeling was detected after exposure to solvent (DMSO) alone (data not shown). Panel J, Q-PCR analysis of *cyp1a* mRNA levels at 72 hpf in solvent-exposed embryos (DMSO) and after exposure to pyrene (PYR), chrysene (CHR), and benz[*a*]anthracene (BAA). Data shown are the mean ± SE derived from three replicate exposure experiments assayed simultaneously on the same plate. Abundance of *cyp1a* mRNA was calculated relative to total template RNA added to the TaqMan assay, based on standard curves produced from the highest (BAA) and lowest (DMSO) samples (see Methods). Raw data were log transformed and analyzed by nested ANOVA ($p<0.001$) and Tukey–Kramer HSD (alpha = 0.05) post hoc. Within each exposure group, some individual biological replicates were statistically different, but means for each group were statistically different from each other across exposures (identified as groups A–D in the Tukey–Kramer HSD test).

Biolabs, Beverly, MA). Final products were visualized on 4% agarose ethidium bromide e-gels (Invitrogen). CYP1A induction was measured by two-step real-time quantitative RT-PCR (Q-PCR) using TaqMan sequence detection chemistry. Total RNA was prepared from three replicate pools of 30 embryos per treatment. Template RNA concentrations were quantified with the NanoDrop spectrophotometer, and the samples were diluted to the same concentration prior to the RT reaction. Probes and primers for Q-PCR assays were designed according to sequence data using Primer Express software from Applied Biosystems (ABI, Carson City, CA). For each RNA preparation, a sample was analyzed without RT reaction to test for DNA contamination and without reverse transcriptase to test for component purity. The CYP1A primer/probe set was 5′-TGGAGAG-CACGCCGAAAG-3′ (forward), 5′-CCCTGCACCGTTGAAAATGT-3′ (reverse), and FAM-5′-TGGCGCTCAATGCCCTGCG-3′-TAMRA (probe). Zebrafish β-actin was used as an internal control to normalize mRNA abundance. The β-actin primer/probe set (Trant et al., 2001) was 5′-AGGTCATCAC-CATCGGCAAT-3′ (forward), 5′-GATGTCCACGTCGCACTTCAT-3′ (reverse), and FAM-5′-CTTCCAGCCTTCCTTCCTGGGTATGGAA-3′-TAMRA (probe). Assays were run on an ABI 7700 Sequence Detector using 96-well plates and ABI's Universal PCR MasterMix Reagent. PCR efficiency was measured using a serial dilution of a positive control RNA sample (benz[*a*]

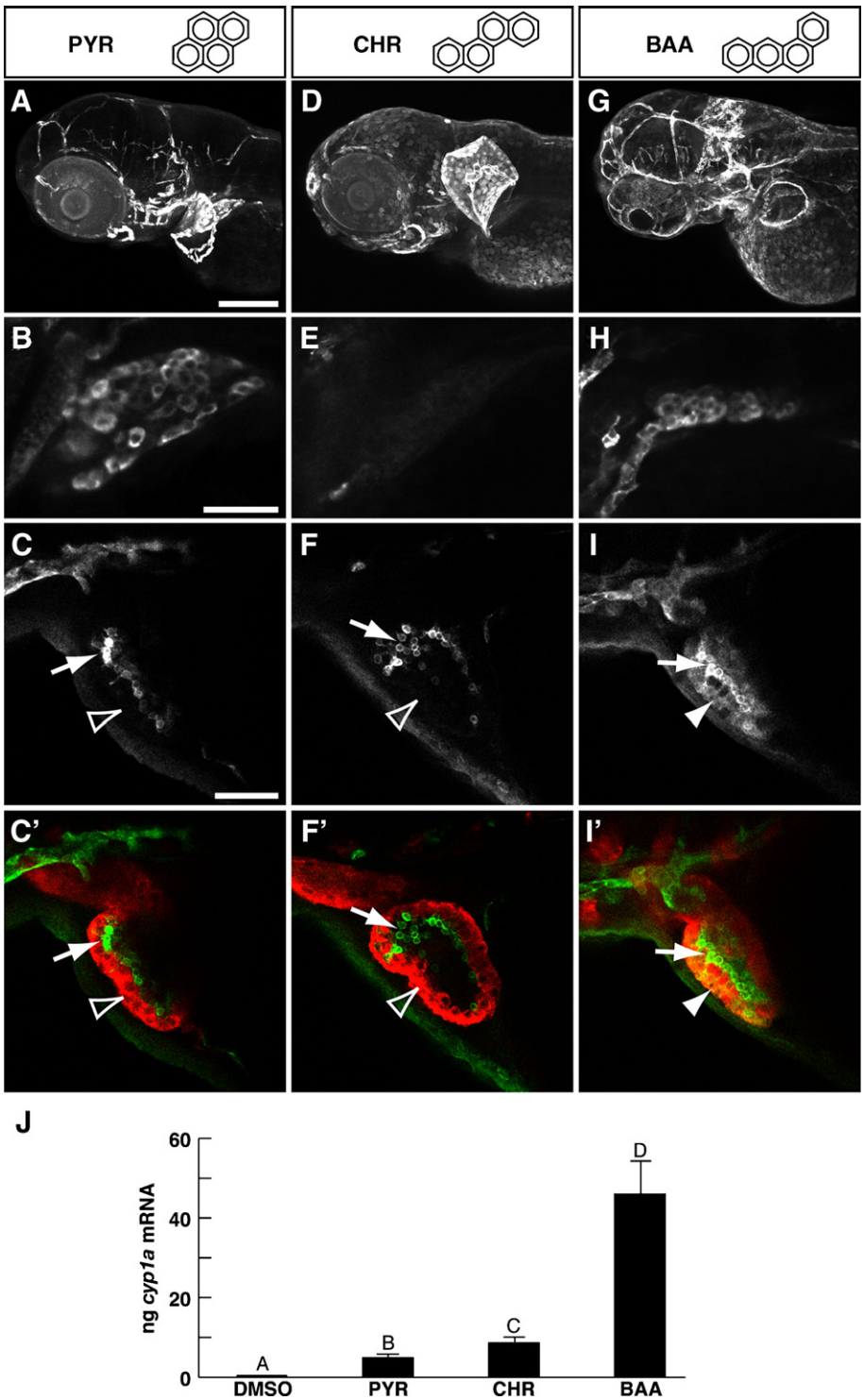

anthracene-exposed embryos) from within the experiment as a reference. Three technical replicates were run for standard curve dilutions and each sample. Reaction conditions were as follows for 25 μl PCRs: 12.5 μl of Universal PCR MasterMix (ABI), 0.5 μl of forward primer (45 mM stock), 0.5 μl of reverse primer (45 mM stock), 0.5 μl of probe (10 mM stock), 8.0 μl ddH_2O, and 3.0 μl of 1:10 diluted RT reaction. Cycling parameters were: 50 °C for 2 min, 95 °C for 10 min and 40 cycles of 95 °C for 15 s followed by 60 °C for 1 min. Because pyrene exposure reduced β-actin transcript abundance, CYP1A transcript abundance was calculated using threshold cycle values relative to the standard curves and expressed as *n*-fold abundance over the 1× calibrator sample (DMSO-exposed embryos).

Imaging of live embryos/larvae, immunofluorescence, confocal microscopy, and histology. Digital still micrographs were obtained and videomicroscopy of live embryos and larvae performed as described previously (Incardona et al., 2004). To quantify pericardial edema, lateral images were obtained for at least 14 embryos/larvae mounted in 3% methylcellulose, and the pericardial area measured in pixels by tracing the boundaries of the pericardial space in NIH ImageJ. Pixel area was converted to μm^2 based on the calibrated magnification. Antibodies used for immunofluorescence were anti-fish CYP1A mouse monoclonals 1-12-3 (Park et al., 1986) and C10-7 (Myers et al., 1993) (Cayman Chemical, Ann Arbor, MI) and anti-myosin heavy chain monoclonal MF20 (Bader et al., 1982) (Developmental Studies Hybridoma Bank, University of Iowa). Embryos were fixed 3 h to overnight in 4% phosphate-buffered paraformaldehyde and processed for immunofluorescence as described previously (Incardona et al., 2004; Incardona et al., 2005). Secondary antibodies (Invitrogen-Molecular Probes, Eugene, OR) were AlexaFluor488-conjugated goat-anti-mouse IgG (mAb C10-7) or IgG1 (mAb 1-12-3) and AlexaFluor568-conjugated goat anti-mouse IgG2b (MF20). Immunolabeled embryos were mounted in 3% methylcellulose and imaged using a Zeiss LSM 5 Pascal confocal system with Ar and HeNe lasers. For histology, larvae were fixed overnight in 4% phosphate-buffered paraformaldehyde and processed for plastic embedding and microtome sectioning as previously described (Linbo et al., 2006).

Results

Waterborne exposure to different tetracyclic AHs results in distinct patterns of CYP1A induction

Exposure of zebrafish embryos to pyrene, chrysene, and benz[*a*]anthracene (Table 1) resulted in qualitatively different patterns of CYP1A induction among tissues and organs. As described previously (Incardona et al., 2004; Incardona et al., 2005), at 72 hpf, exposure to 25 μM pyrene induced CYP1A throughout the vascular endothelium, including the majority of blood vessels in the head (Fig. 1A) and trunk, and in developing hepatocytes (Fig. 1B). Endothelial cells lining the cardiac chambers (i.e. endocardium) also were intensely immunofluorescent for CYP1A, but the myocardium was not (Fig. 1C). Other CYP1A-immunopositive ($CYP1A^+$) tissues included the epithelium of the intestinal bulb and the urinary pore (data not shown). CYP1A immunofluorescence was also detectable just above background in the epidermis. CYP1A immunofluorescence was not observed in other tissues, including skeletal muscle or the central nervous system.

Similarly, as described previously (Incardona et al., 2004; Incardona et al., 2005), exposure to 22 μM chrysene resulted in strong CYP1A induction throughout the epidermis covering the entire larva and in the endothelium of the major blood vessels in the head (Fig. 1D) and trunk. Compared to pyrene, CYP1A induction by chrysene was not as widespread throughout the smaller blood vessels in the brain (see below). Chrysene also induced CYP1A in the endocardium, but not in the myocardium (Fig. 1F). Remarkably, the liver showed no increase over background immunofluorescence in chrysene-exposed larvae (Fig. 1E).

Exposure to 22 μM benz[*a*]anthracene resulted in CYP1A induction in a wider range of tissues. Virtually all of the blood vessels showed intense endothelial CYP1A immunofluorescence, including the minor vessels deep in the brain (Fig. 1G and Fig. S1). While most of the epidermal cells showed CYP1A immunofluorescence at levels similar to chrysene-exposed animals, a band of epidermal cells across the middle of the hindbrain region consistently showed much more intense labeling (Fig. 1G and Fig. S1). The liver, which has an altered morphology in benz[*a*]anthracene-exposed animals (data not shown), showed bright CYP1A immunofluorescence (Fig. 1H). In contrast to both pyrene and chrysene, benz[*a*]anthracene induced CYP1A in both the endocardium and myocardium (Fig. 1I). Moreover, CYP1A immunofluorescence was detected in the skeletal muscle fibers in benz[*a*]anthracene-exposed larvae, as well as in specific cells in both the central and peripheral nervous systems (Fig. S1). In the CNS, ependymal cells at the base of the central canal of the spinal cord and hindbrain were strongly $CYP1A^+$, as were neurons scattered through dorsal regions of the spinal cord. Lateral line neuromasts and glial cells associated with the lateral line nerve were also $CYP1A^+$.

CYP1A induction was also measured for each compound by Q-PCR of CYP1A mRNA at the same time point shown for CYP1A immunofluorescence (Fig. 1J). While CYP1A mRNA levels were negligible in DMSO-exposed embryos at 72 hpf, exposure to 25 μM pyrene resulted in a level of CYP1A mRNA representing a 12-fold induction, chrysene exposure (22 μM) produced a 22-fold induction, and benz[*a*]anthracene exposure (22 μM) produced a 117-fold induction. These levels of total CYP1A mRNA associated with exposure to each PAH generally match the increasing range of tissues showing CYP1A immunoreactivity. These data are also generally consistent with the rank order of AHR potency for these compounds (Table 1) predicted from other studies (Barron et al., 2004b).

Despite relatively robust CYP1A induction, chrysene has no obvious biological effects during embryonic and early larval development of zebrafish, while pyrene and benz[*a*]anthracene produced distinct defects described below. A trivial explanation for lack of chrysene toxicity is simply that the compound has insufficient bioavailability due to its low water solubility, as predicted by narcosis models. If this is the case, then benz[*b*]anthracene should be similarly nontoxic (Table 1). However, benz[*b*]anthracene exposure resulted in complex dose-dependent toxicity evident by 48 hpf, including mortality at 8–10 μM, and developmental defects at 2–6 μM including failure of head straightening, lack of finfold development, and poor cardiac looping with pericardial edema and hemorrhage (Fig. S2). These concentrations of benz[*b*]anthracene produced a pattern of CYP1A immunofluorescence that overlapped considerably

with that from benz[*a*]anthracene exposure, including the myocardium (Fig. S2). The complexities of benz[*b*]anthracene toxicity require a more detailed analysis to be described elsewhere.

Systemic larval toxicity of pyrene is partially dependent on hepatic CYP1A metabolism

Continuous exposure to pyrene (beginning soon after fertilization) at doses above 5 μM resulted in a syndrome of systemic toxicity that appears in early larval stages (i.e. at ~96 hpf) (Incardona et al., 2004; Incardona et al., 2005). The visible signs of pyrene toxicity included dorsal curvature of the body axis, reduced peripheral circulation, anemia, pericardial edema that evolves into yolk sac edema, and cell death beginning in the brain and later involving the spinal cord. At these stages (and prior), CYP1A induction was evident throughout the vascular endothelium and the liver. Pyrene-exposed larvae began to die during the fifth day, a time coincident with changes in the appearance of the liver (Figs. 2A, B). Grossly, the liver of pyrene-exposed larvae appeared opaque with irregular margins. Histologically, the liver was not necrotic but appeared congested with enlarged vacuolated hepatocytes possibly indicative of either swollen mitochondria or endoplasmic reticulum (Figs. 2A, B).

Although pyrene toxicity can be prevented or delayed by knockdown of *ahr2* or *cyp1a* (Incardona et al., 2005), *ahr1a* was expressed at levels that are much higher in the liver than any other tissue (Andreasen et al., 2002). We therefore tested whether *ahr1a* knockdown would influence pyrene toxicity. Injection of *ahr1a*-MO targeting the exon 2–intron 2 (E2I2) splice donor site resulted in an aberrantly spliced transcript derived from a cryptic splice site in exon 2. This introduced a unique *Hpa*I site into the cDNA product, and a frame shift leading to a stop codon just before helix 2 of the AHR1A bHLH domain, (Fig. 2C). Embryos injected with control morpholinos and exposed to 25 μM pyrene showed liver abnormalities, pericardial edema (Fig. 2E), and dorsal curvature after 96 hpf. At the same time point, *ahr1a* morphants exposed to pyrene showed signs of pyrene resistance, including a normal liver and absence of pericardial edema (Fig. 2D) and neural tube cell death (data not shown). The mean pericardial areas determined from lateral images for control embryos or *ahr1a* morphants exposed to pyrene were 370 ± 19 μm^2 and 256 ± 10 μm^2 ($n = 17$ each, *t*-test $p < 0.001$), respectively. Dorsal curvature was not

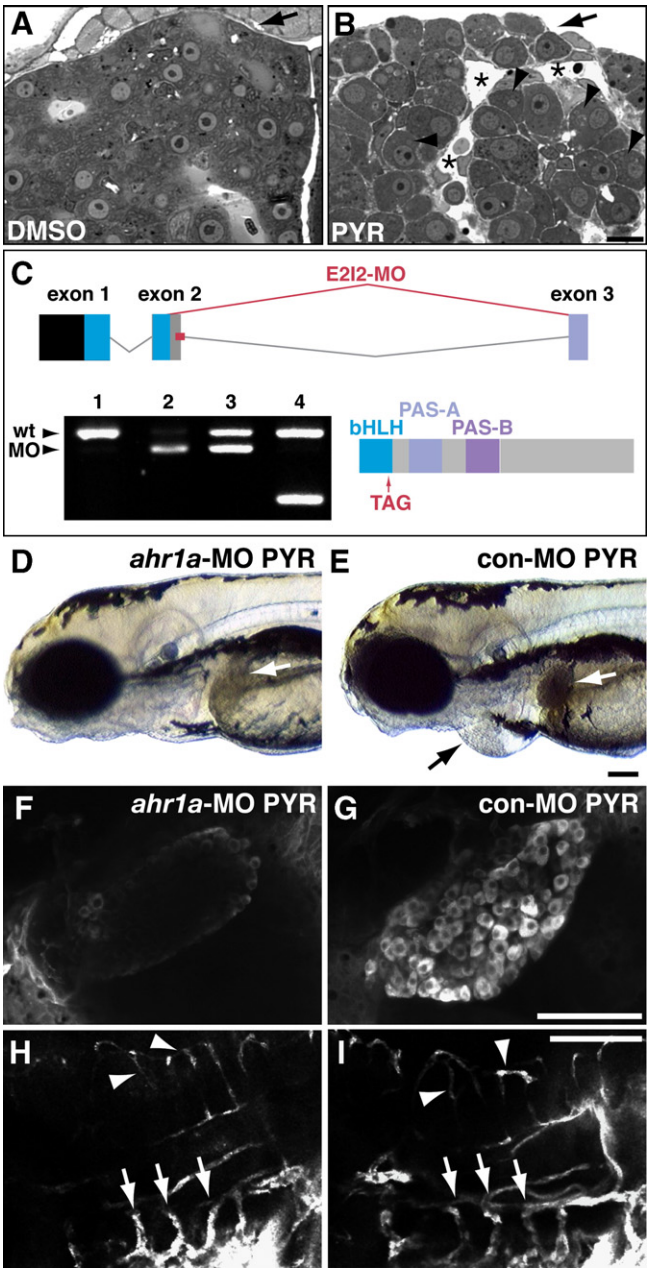

Fig. 2. Knockdown of *ahr1a* prevents pyrene toxicity and hepatic CYP1A induction. Embryos were injected with *ahr1a* or control MOs and exposed to 25 μM pyrene or solvent (DMSO) from 6 to 96 hpf. Larvae were fixed and processed for histology (A, B), imaged live (D, E), or fixed and processed for CYP1A immunofluorescence (F–I). Transverse sections of the liver are shown (A, B), in all other images anterior is at left and dorsal at top; scale bars are 10 μm (A, B) and 100 μm (D–I). Panel A, liver in DMSO-exposed larva with smooth capsule (arrow) and normal hepatocytes with typical polygonal shape. Panel B, liver in pyrene-exposed larvae shows a scalloped capsule (arrow) due to cell swelling, larger rounded hepatocytes often containing vacuoles (arrowheads), and increased intercellular spaces and enlarged sinuses (asterisks) consistent with congestion. Images are representative of 6 larvae sectioned for each treatment. Panel C, MO targeting *ahr1a* exon 2–intron 2 splice donor site causes a cryptic splicing event (*E2I2-MO*, indicated in red) that results in a smaller PCR product and introduces a unique *Hpa*I site and TAG stop codon upstream of helix 2 of the bHLH domain. RT-PCR analysis showed only wild type (wt) transcript in uninjected embryos (lane 1), predominantly morphant (MO) cryptic splice product in injected embryos by 48 hpf (lane 2), with wt transcript increasing by 96 hpf (lane 3); morphant transcript contains a unique *Hpa*I site not present in wt (lane 4). Panel D, pyrene-exposed *ahr1a* morphant with a normally translucent liver and no pericardial edema. Panel E, pericardial edema (black arrow) and opaque liver with irregular margins (white arrow) in a larva injected with control MO and exposed to pyrene. Images are representative of at least 20 larvae from each of three replicate experiments. Panel F, reduced CYP1A immunofluorescence in hepatocytes of a pyrene-exposed *ahr1a* morphant compared to larva injected with control MO, panel G. Panel H, CYP1A immunofluorescence in the branchial arches (arrows) and neural vessels (arrowheads) of a pyrene-exposed *ahr1a* morphant compared to a control pyrene-exposed larva, panel I.

EX5049-000006-TRB

prevented in *ahr1a* morphants (data not shown), and as previously observed for *cyp1a* morphants (Incardona et al., 2005), *ahr1a* morphants ultimately succumbed to pyrene toxicity with a delay of 18–24 h (data not shown).

Consistent with the known expression pattern of *ahr1a* (Andreasen et al., 2002), immunofluorescent analysis of CYP1A expression showed a specific reduction in hepatic CYP1A in *ahr1a* morphants exposed to pyrene (Fig. 2F) relative to larvae injected with control morpholinos (Fig. 2G). There was no effect of *ahr1a*-MO on the extensive vascular endothelial CYP1A induction associated with pyrene exposure (Fig. 2H) compared to controls (Fig. 2I). These findings indicate that hepatic CYP1A activity contributes strongly to the systemic toxicity of pyrene, most likely through the production of a toxic metabolite. It is possible that the metabolism of pyrene by CYP1A in the vascular endothelium contributes to some of the effects, in particular, dorsal curvature.

Cardiac toxicity of benz[a]anthracene requires AHR2 function in the myocardium, but is independent of CYP1A induction

Exposure to 22 μM benz[*a*]anthracene resulted in cardiovascular defects by 48 hpf that were distinct from the effects of both the other tetracyclic AHs and cardiotoxic tricyclic AHs (Incardona et al., 2004; Incardona et al., 2005). Benz[*a*]anthracene-exposed embryos appeared normal through 32 hpf, but by 48 hpf showed failure to complete cardiac looping with concomitant pericardial edema (see Web Movie 1). A high percentage of embryos had intracranial hemorrhage (Table 2, and Fig. 3G). By 72 hpf, benz[*a*]anthracene-exposed embryos showed more severe edema involving the yolk sac, mild dorsal curvature, and relative to solvent-exposed embryos (Fig. 3A), reduced body length, eyes, and jaw cartilages (Fig. 3B and data not shown). Cardiac structure (Figs. 3D, F) and function (Web Movie 1) were dramatically altered, with incomplete looping and reduction of both cardiac chambers. Pericardial edema is probably secondary to reduced cardiac output. Between 48 and 72 hpf, the zebrafish ventricular myocardium undergoes proliferation and the wall thickens from 1 cell to 4 cells wide (Hu et al., 2000; Rottbauer et al., 2001) (Fig. 3E). In benz[*a*]anthracene-exposed embryos, the myocardium failed to proliferate, and degenerative changes were observed in ventricular cardiomyocytes (Fig. 3F).

Table 2
Benz[*a*]anthracene-induced cardiovascular defects are AHR2-dependent and CYP1A-independent

Treatment	Percent intracranial hemorrhage at 48 hpf	Percent pericardial edema at 72 hpf
Uninjected+44 μM benz[*a*]anthracene	37 (n=83)	100 (n=67)
Control MO+44 μM benz[*a*]anthracene	50 (n=74)	100 (n=59)
ahr2-MO+44 μM benz[*a*]anthracene	4 (n=144)	7 (n=132)
cyp1a-MO+44 μM benz[*a*]anthracene	48 (n=63)	100 (n=34)
Uninjected+DMSO	0 (n=40)	0 (n=36)
Control MO+DMSO	0 (n=47)	0 (n=41)
ahr2-MO+DMSO	1 (n=71)	2 (n=50)
cyp1a-MO+DMSO	0 (n=30)	0 (n=24)

Embryos were injected with indicated morpholinos and exposed as described under Experimental Procedures, and scored for the presence of intracranial hemorrhage at 48 hpf and pericardial edema at 72 hpf. Data shown are from a single experiment that is representative of four experiments. Some embryos were removed from each group at 48 hpf and fixed for immunofluorescence.

The cardiac effects of benz[*a*]anthracene are remarkably similar to the AHR2-dependent effects of TCDD (Antkiewicz et al., 2005). Consistent with this, *ahr2* morphants were resistant to benz[*a*]anthracene-mediated cardiovascular toxicity (Fig. 4 and Table 2). Embryos injected with control morpholino (Fig. 4, bar 3) showed the same degree of pericardial edema as uninjected controls (Fig. 4, bar 2) at 48 hpf after exposure to 44 μM benz[*a*]anthracene. In contrast, *ahr2* morphants exposed to benz[*a*]anthracene showed no pericardial edema (Fig. 4, bar 4) and had a mean pericardial area not significantly different than unexposed embryos (Fig. 4, bar 1). Unlike the case with pyrene exposure, *cyp1a* knockdown did not prevent benz[*a*]anthracene-induced pericardial edema. Similar results were observed for benz[*a*]anthracene-induced intracranial hemorrhage (Table 2). Injection of *ahr2*-MO largely prevented the occurrence of intracranial hemorrhage, whereas injection of control-MO or *cyp1a*-MO did not. However, although the degree of pericardial edema in *cyp1a* morphants was not significantly higher (Fig. 4, bar 5), the embryos appeared to be more severely impacted as suggested by an increased number with yolk sac edema (data not shown). This suggests that metabolism of benz[*a*]anthracene by CYP1A may provide a mild protective effect.

As shown in Fig. 1, uninjected embryos (Figs. 5A, D) or embryos injected with control morpholino (Fig. 5B) showed robust CYP1A immunofluorescence in both the endocardium and myocardium, as well as the epidermis. Remarkably, in conjunction with normal cardiac development in *ahr2* morphants, CYP1A induction was blocked specifically in the myocardium and the epidermis (Fig. 5C), but the endocardial and other vascular endothelial CYP1A induction were intact (Fig. 5C and data not shown). This pattern is similar to that observed for chrysene exposure, where *ahr2* knockdown selectively blocks epidermal but not vascular endothelial CYP1A induction (Incardona et al., 2005). Presumably, AHR1A or AHR1B mediates endocardial and vascular endothelial CYP1A induction in *ahr2* morphants. Embryos injected with *cyp1a*-MO that were not protected from benz[*a*]anthracene cardiotoxicity showed an absence of immunodetectable CYP1A in the heart (Fig. 5E). These findings indicate that benz[*a*]anthracene impacts cardiac development in an AHR2-dependent, CYP1A-independent manner, much like TCDD. Moreover, AHR2 activation in the myocardium is required for toxicity, while endocardial CYP1A induction (or AHR pathway activation) has little apparent effect on early heart development.

Tissue uptake and distribution of tetracyclic AHs are differentially dependent on circulation

To begin to address the factors that determine the different patterns of CYP1A induction associated with exposure to pyrene, chrysene, and benz[*a*]anthracene, we first explored a

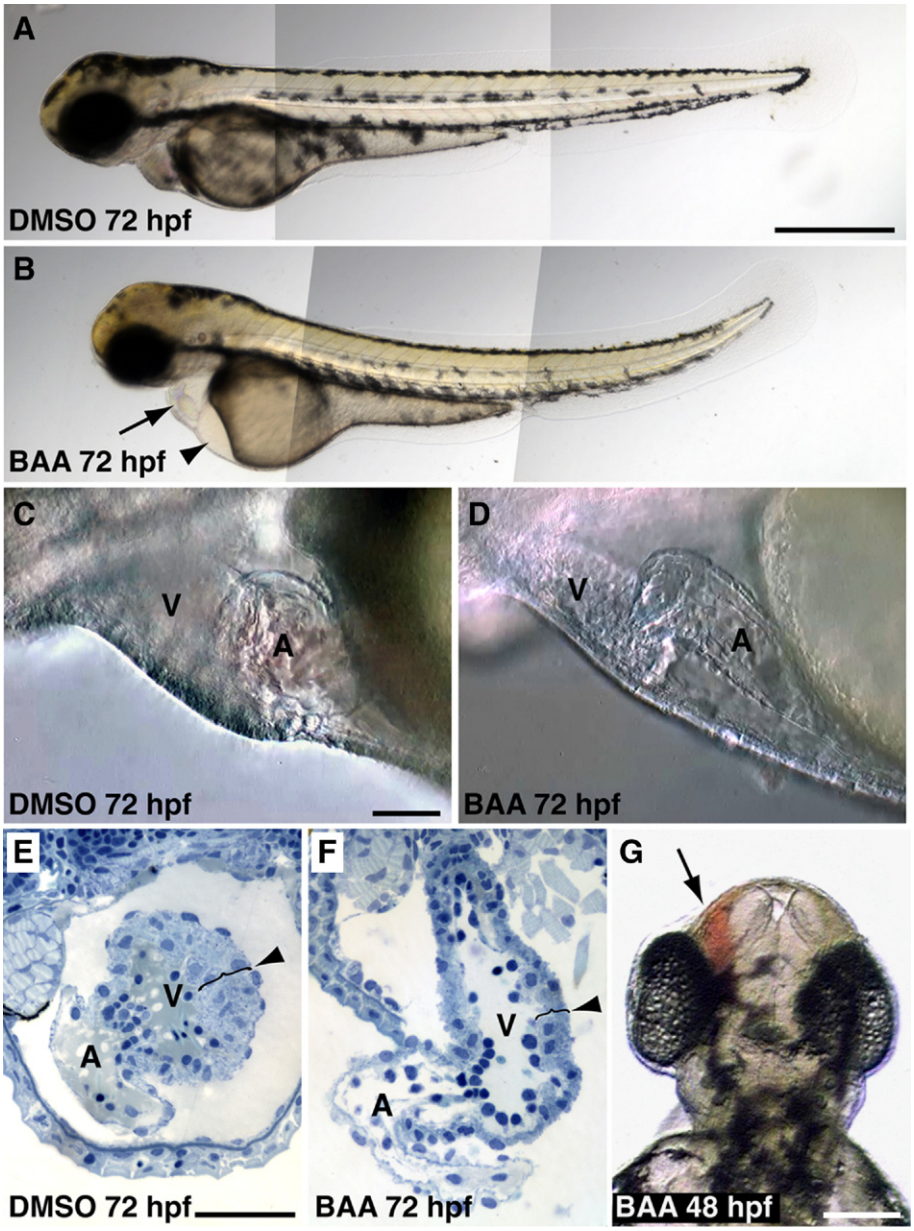

Fig. 3. Exposure to benz[*a*]anthracene (BAA) results in cardiovascular defects. Embryos were exposed to 22 μM benz[*a*]anthracene or solvent (DMSO) from 6 to 72 hpf and imaged live at the indicated time (A–D, G) or fixed and processed for histological analysis of cardiac tissue (E, F). Shown are lateral views with anterior to the left and dorsal at top (A–D), transverse sections with dorsal at top (E, F) and dorsal view with anterior at top (G); scale bars are 0.5 mm (A, B), 50 μm (C, D), 20 μm (E, F), and 0.2 mm (G). Panel A, normal DMSO-exposed larva at 72 hpf. Panel B, benz[*a*]anthracene-exposed larva with pericardial (arrow) and yolk sac (arrowhead) edema, intracranial hemorrhage, and dorsal curvature of the body axis. Panel C, higher magnification of normal heart in a DMSO-exposed larva (*V*, ventricle; *A*, atrium). Panel D, poorly looped heart with small, stiff ventricle in a larva exposed to benz[*a*]anthracene. Panel E, section of a normal heart with a thickened ventricle wall up to 4 cells wide (bracket and arrowhead). Panel F, section of heart in a benz[*a*]anthracene-exposed larva with a thin, elongated ventricle only 1–2 cells wide (bracket and arrowhead). Panel G, left-sided intracranial hemorrhage (arrow) in a benz[*a*]anthracene-exposed larva.

role for a functional circulation. Due to their small size, zebrafish embryos can obtain sufficient oxygen by diffusion and do not require circulation until the early larval period (Rombough, 2002). If fish tissues take up PAHs by passive diffusion, as assumed by narcosis models, then circulation should not be required to achieve internal levels resulting in CYP1A induction. An effective means for generating embryos that never develop circulation is by knockdown of the cardiac-specific isoform of troponin T, encoded by the zebrafish *silent heart* (*sih*) locus (Sehnert et al., 2002). Injection of *sih*-MO readily phenocopies the *sih* null mutant, and morphants do not establish a heartbeat due to disorganized sarcomeres in cardiac muscle (Sehnert et al., 2002).

In uninjected embryos exposed to pyrene (25 μM), CYP1A immunofluorescence was strong throughout the vasculature, as shown for the head (Fig. 6A) and trunk (Fig. 6B) by epifluorescent imaging. Confocal imaging close to the midline of the brain demonstrated strong CYP1A immunofluorescence in a subset of the deep neural vessels (Fig. 6C). In contrast, *sih* morphants exposed to pyrene in parallel showed very low

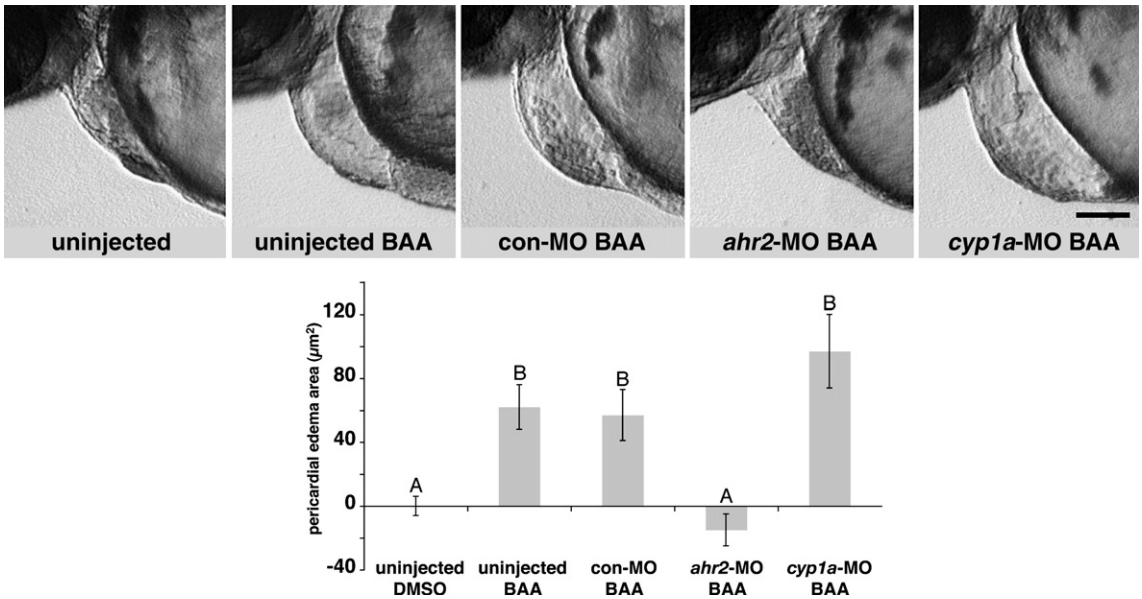

Fig. 4. Benz[*a*]anthracene cardiac toxicity is AHR2-dependent and CYP1A-independent. Uninjected embryos or embryos injected with control, *ahr2*, or *cyp1a* MOs were exposed to 22 μM benz[*a*]anthracene from 6 to 48 hpf and scored for pericardial edema. Pericardial area was measured in lateral images, and the mean area in uninjected DMSO-exposed control embryos (i.e. no edema) was subtracted from individual measurements to give an estimate of the degree of pericardial edema. Data represent the mean ± SE ($n = 14–16$) obtained after subtraction of the mean control area and were analyzed by one-way ANOVA ($p < 0.0001$) and Tukey–Kramer HSD (alpha = 0.05) post hoc. Groups A and B were statistically different. For each bar in the plot, a representative corresponding image is shown above. Scale bar is 50 μm.

CYP1A immunofluorescence, particularly in superficial vessels of the branchial arches (Fig. 6D) and tail (Fig. 6E). Moreover, CYP1A induction was not observed in the deep neural vessels (Fig. 6F). Uninjected embryos exposed to chrysene (22 μM) consistently showed strong CYP1A induction in both the epidermis and vasculature, as observed in the head and trunk by epifluorescent imaging (Figs. 6G and H, respectively). As observed for pyrene, confocal imaging near the midline of the brain demonstrated strong CYP1A immunofluorescence in the deep neural vessels, but a different subset (Fig. 6I). In contrast, *sih* morphants exposed to chrysene showed a markedly higher level of CYP1A immunofluorescence in the epidermis (Figs. 6J and K), but an absence of induction in the deep neural vessels (Fig. 6L). In marked contrast to the results obtained with pyrene and chrysene, the widespread vascular CYP1A immunofluorescence observed in uninjected embryos (Figs. 6M, N, and O) exposed to benz[*a*]anthracene (22 μM) was unaffected by *sih* knockdown. Although benz[*a*]anthracene-exposed *sih* morphants showed higher epidermal CYP1A immunofluorescence (Figs. 6P, Q), strong induction was evident in the deep neural vessels (Fig. 6R). As an independent means to stop circulation after it is well established, embryos were treated at 36 hpf with 40 mM 2,3-butanedione monoxime (Serluca et al., 2002), which stops cardiac function by inhibiting myofibrillar ATPase (Herrmann et al., 1992). After circulation ceased (~15 min), embryos were maintained in 20 mM 2,3-butanedione monoxime and exposed to each tetracyclic PAH until 50 hpf. Similar results for the patterns of CYP1A induction observed in *sih* morphants were obtained with chrysene (data not shown), but the combinations of pyrene and benz[*a*]anthracene with 2,3-butanedione monoxime were lethal, with widespread cytotoxicity evident by 50 hpf. These findings strongly suggest that circulation is required to deliver pyrene and chrysene to internal tissues, but that benz[*a*]anthracene can diffuse or is transported to internal tissues in a circulation-independent or passive manner.

Discussion

In conjunction with our previous work (Incardona et al., 2004; Incardona et al., 2005), we have identified three distinct modes of action leading to unique syndromes of developmental toxicity in fish embryos exposed to different PAHs. We demonstrated previously that tricyclic AHs and weathered ANS crude oil cause early cardiac dysfunction during key stages of cardiac morphogenesis. These effects are independent of the AHR and are most likely secondary to impacts on cardiac ion channels or other targets involved in the cardiac conduction system (Incardona et al., 2004; Incardona et al., 2005). Indeed, in the case of tricyclic AHs, the AHR pathway provides modest protection as *ahr1a*/*ahr2* and *cyp1a* morphants showed higher sensitivity to these compounds. The results presented here indicate that, as more potent AHR agonists, some tetracyclic AHs (pyrene and benz[*a*]anthracene) produce developmental toxicity through the AHR pathway. Nevertheless, even among the AHR agonists tested here, there are different mechanisms of AHR-dependent toxicity, and toxicity cannot be predicted by receptor activation potency alone.

First, the cardiovascular toxicity of benz[*a*]anthracene overlaps considerably with that of TCDD. Both TCDD and benz[*a*]anthracene cause reduced proliferation of ventricular cardiomyocytes and defects in cardiac looping during the same

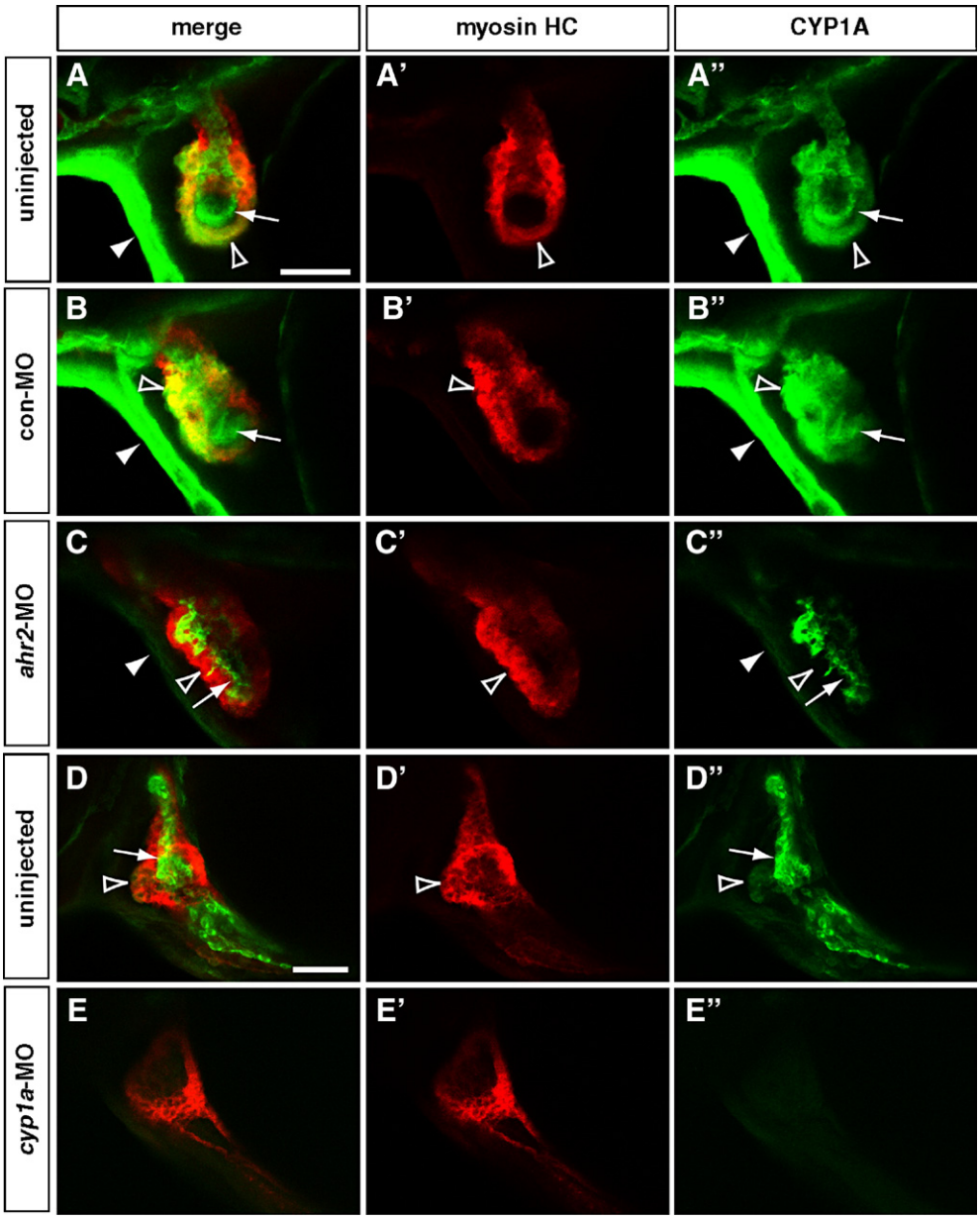

Fig. 5. Myocardial but not endocardial AHR activation is required for benz[*a*]anthracene cardiac toxicity. Uninjected embryos or embryos injected with control, *ahr2*, or *cyp1a* MOs were exposed to 22 μM benz[*a*]anthracene from 6 to 48 or 72 hpf then fixed and processed for CYP1A (green) and myosin heavy chain (red) immunofluorescence. Representative lateral confocal sections are shown, with anterior to the left and dorsal at top. Merged images are shown in the first column, with individual channels for myocardial myosin and CYP1A in the second and third columns, respectively. Filled arrowheads indicate epithelium over the pericardium, unfilled arrowheads indicate the myocardium, and arrows indicate $CYP1A^{+}$ endocardium; scale bars are 50 μm (A–C and D, E). Panel A, uninjected embryo exposed to benz[*a*]anthracene to 72 hpf. Panel B, embryo injected with control-MO and exposed to benz[*a*]anthracene to 72 hpf. Panel C, *ahr2* morphant exposed to benz[*a*]anthracene to 72 hpf. Panel D, uninjected embryo exposed to benz[*a*]anthracene to 48 hpf. Panel E, *cyp1a* morphant exposed to benz[*a*]anthracene to 48 hpf.

developmental stages (48–72 hpf) (Antkiewicz et al., 2005). In contrast to the tricyclic AHs, but similar to TCDD, the defects in cardiac function and morphogenesis induced by benz[*a*]anthracene are AHR2-dependent and CYP1A-independent. Moreover, the looping and proliferative defects caused by benz[*a*]anthracene require AHR2 activation in the myocardium, implying that AHR activation may disrupt (directly or indirectly) the normal program of cardiomyocyte gene expression during these key phases of ventricular maturation. These results have important implications for proposed mechanisms of TCDD toxicity. Previous studies have focused on the contribution of vascular endothelial AHR activation (or CYP1A induction) to the edematous syndrome associated with exposure of fish embryos to TCDD (Cantrell et al., 1996; Guiney et al., 1997; Cantrell et al., 1998; Guiney et al., 2000; Dong et al., 2002). However, the robust endocardial and vascular endothelial CYP1A expression observed in AHR2 morphants protected from benz[*a*]anthracene toxicity indicates that endothelial AHR activation is insufficient for disruption of cardiac morphogenesis. This is further supported by the lack of cardiac defects

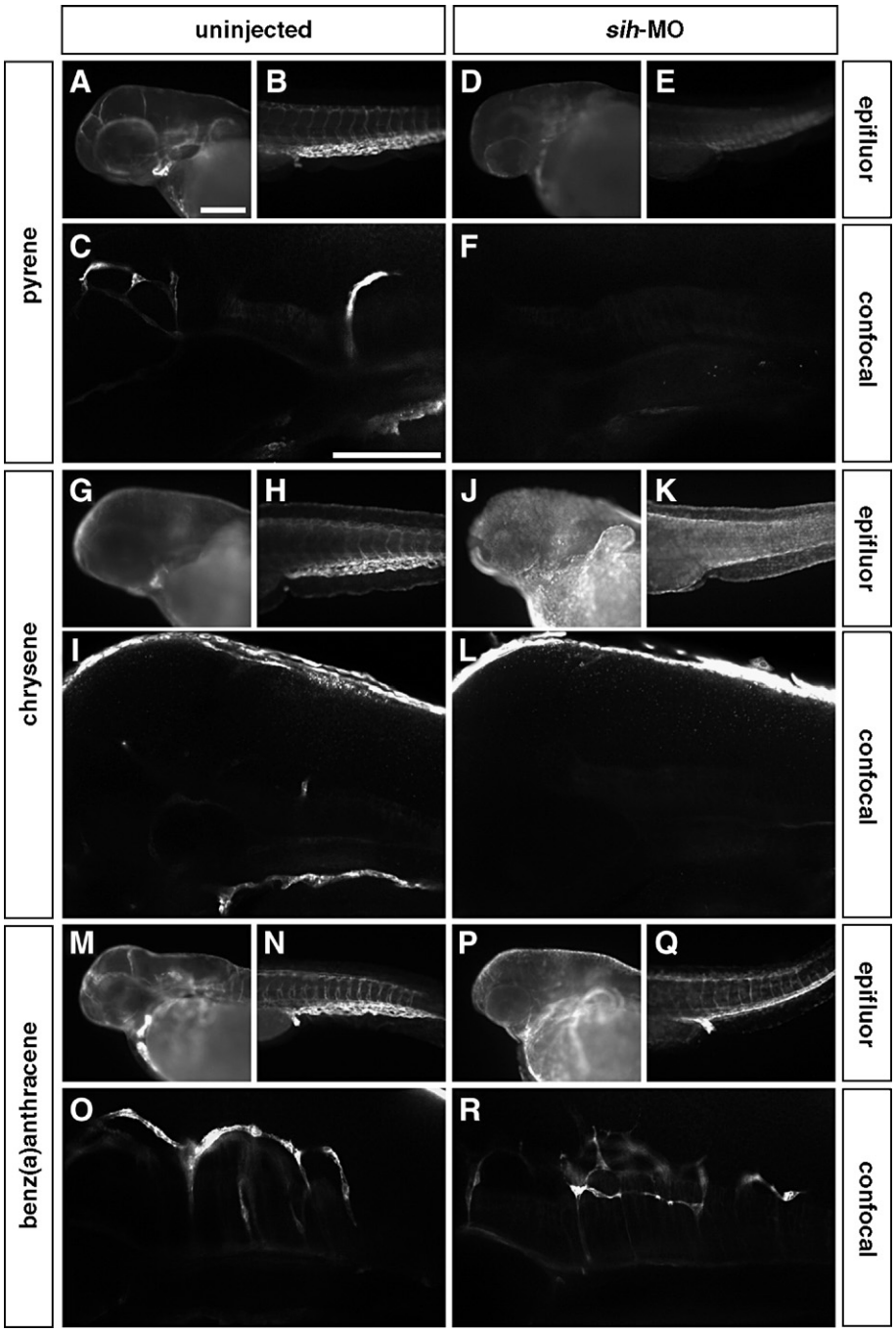

Fig. 6. Tissue-specific patterns of CYP1A induction by tetracyclic AHs are differentially dependent on circulation. Uninjected embryos or *silent heart* (*sih*) morphants were exposed to pyrene (25 μM), chrysene (22 μM), or benz[*a*]anthracene (22 μM) from 6 to 72 hpf then fixed and processed for CYP1A immunofluorescence. Shown are representative lateral epifluorescent images of the head (A, D, G, J, M, and P) and trunk (B, E, H, K, N, and Q) and higher magnification lateral confocal sections taken adjacent to the midline and spanning the midbrain–hindbrain junction (C, F, I, L, O, and R). Anterior is to the left and dorsal at top in all images; scale bars in panels A and C are 100 μm and representative for all epifluorescent and confocal images, respectively. Panels A–C, uninjected larva exposed to pyrene. Panels D–F, *sih* morphant exposed to pyrene. Panels G–I, uninjected larva exposed to chrysene. Panels J–L, *sih* morphant exposed to chrysene. Panels M–O, uninjected larva exposed to benz[*a*]anthracene. Panels P–R, *sih* morphant exposed to benz[*a*]anthracene. Epifluorescent images are representative of at least 15 larvae and confocal images representative of 6 larvae for each compound.

in embryos exposed to pyrene or chrysene despite robust expression of CYP1A in the endothelium.

Second, pyrene exposure results in a very different syndrome of systemic toxicity in which the heart is not a primary target, and by which hepatic CYP1A induction plays a major role. The previously observed pyrene resistance of *cyp1a* morphants (Incardona et al., 2005) and the protection provided by selective reduction in hepatic CYP1A induction in *ahr1a* morphants strongly suggest that pyrene toxicity results from a product of hepatic metabolism that reaches the systemic circulation.

Alternatively, the systemic effects of pyrene exposure could result from altered liver function secondary to CYP1A-mediated pyrene hepatotoxicity.

These findings also have important implications for structure–function relationships among AHR isoforms. Based on *in vitro* studies with TCDD and other potent dioxin-like AHR ligands, zebrafish AHR1A appeared to be an inactive receptor (Andreasen et al., 2002), and it has been suggested that *ahr1a* is an incipient pseudogene (Karchner et al., 2005). However, our data are consistent with the ability of PAH ligands to activate CYP1A transcription *in vivo* through AHR1A. It is unlikely that a translation product of the *ahr1a*-MO cryptic splice acts as a dominant negative to AHR2 because both helices of the bHLH domain are required for dimerization (Fukunaga et al., 1995). Nevertheless, in conjunction with our previous findings that *ahr2*-MO both prevents pyrene toxicity and blocks CYP1A induction in the liver and throughout the vascular endothelium (Incardona et al., 2005), these results suggest that there may be complex interactions or relationships among the fish AHR isoforms that differ from the canonical single-isoform AHR pathway in mammals and merit further exploration.

The toxicity of dioxins and planar polychlorinated biphenyls correlates well with affinity of AHR binding or efficacy of receptor activation (Safe, 1990; Hestermann et al., 2000). Under the assumption that PAHs act similarly, a toxic equivalency approach has been used to predict AHR-mediated PAH toxicity. While this approach may be justified when considering carcinogenic potential (mediated by AHR activation and CYP1A metabolism), our findings indicate that this approach fails to predict early life stage toxicity in fish. Although our Q-PCR results suggest that the potencies of pyrene and chrysene for AHR activation in zebrafish are closer than predicted by other systems (Barron et al., 2004b), this most likely reflects toxicokinetic differences (i.e. the higher water solubility of pyrene). Nevertheless, this type of model would still predict that chrysene should be more toxic than pyrene, yet chrysene has no discernable impact on developing zebrafish through at least 5 days post-fertilization, despite robust CYP1A induction. Moreover, these studies indicate that the specific tissues impacted by AHR activation are more relevant than overall levels of pathway activation. The tissue-specific patterns of CYP1A induction and potential requirement of active circulation-associated processes to achieve these patterns strongly suggest that individual PAHs have complex toxicokinetics. Although it is possible that there are other impacts on the development of vascular endothelial cells that are secondary to loss of circulation that might prevent CYP1A induction by pyrene or chrysene, the normal development of the embryonic vasculature in *sih* and other cardiac mutants (Isogai et al., 2003) suggests that this is unlikely. These findings, in conjunction with the observed toxicity of benz[*b*]anthracene relative to chrysene, do not support models that assume lipids are non-specific targets for PAHs, resulting in narcotic-like toxicity (Di Toro and McGrath, 2000; Di Toro et al., 2000; French-McCay, 2002).

In summary, this analysis of tetracyclic AH developmental toxicity, combined with previous studies on tricyclic PAHs, demonstrates that widely accepted models of PAH toxicity are oversimplified and will therefore fail to accurately predict many aspects of PAH biological activity. PAHs historically have been treated as a common class of compounds, but should be considered as individual compounds or subfamilies of compounds with specific activities. It is clear from these results that predicting the toxicity of complex PAH mixtures will be more difficult than previously anticipated. However, they also underscore an urgent need for expanded research efforts on these ubiquitous contaminants whose inputs into the environment will only increase in the foreseeable future.

Acknowledgments

This work was funded by the NOAA Coastal Storms Program and Oceans and Human Health Initiative and a grant to J.P.I. and N.L.S. from the California Department of Fish and Game's Oil Spill Response Trust Fund administered through the Oiled Wildlife Care Network, School of Veterinary Medicine, University of California, Davis. No funding source was involved in the design or implementation of the studies described herein. We thank Tiffany Linbo for excellent fish husbandry, Carla Stehr for assistance with histology, Jon Dickey for assistance with Q-PCR assays, David Baldwin for advice on statistical analysis, and Jim Meador and Penny Swanson for critical reviews of the manuscript.

Appendix A. Supplementary Data

Supplementary data associated with this article can be found, in the online version, at doi:10.1016/j.taap.2006.09.018.

References

Abnet, C.C., Tanguay, R.L., Hahn, M.E., Heideman, W., Peterson, R.E., 1999a. Two forms of aryl hydrocarbon receptor type 2 in rainbow trout (*Oncorhynchus mykiss*). Evidence for differential expression and enhancer specificity. J. Biol. Chem. 274, 15159–15166.

Abnet, C.C., Tanguay, R.L., Heideman, W., Peterson, R.E., 1999b. Transactivation activity of human, zebrafish, and rainbow trout aryl hydrocarbon receptors expressed in COS-7 cells: greater insight into species differences in toxic potency of polychlorinated dibenzo-*p*-dioxin, dibenzofuran, and biphenyl congeners. Toxicol. Appl. Pharmacol. 159, 41–51.

Andreasen, E.A., Hahn, M.E., Heideman, W., Peterson, R.E., Tanguay, R.L., 2002. The zebrafish (*Danio rerio*) aryl hydrocarbon receptor type 1 is a novel vertebrate receptor. Mol. Pharmacol. 62, 234–249.

Antkiewicz, D.S., Burns, C.G., Carney, S.A., Peterson, R.E., Heideman, W., 2005. Heart malformation is an early response to TCDD in embryonic zebrafish. Toxicol. Sci. 84, 368–377.

Bader, D., Masaki, T., Fischman, D.A., 1982. Immunochemical analysis of myosin heavy chain during avian myogenesis in vivo and in vitro. J. Cell Biol. 95, 763–770.

Barron, M.G., Carls, M.G., Heintz, R., Rice, S.D., 2004a. Evaluation of fish early life-stage toxicity models of chronic embryonic exposures to complex polycyclic aromatic hydrocarbon mixtures. Toxicol. Sci. 78, 60–67.

Barron, M.G., Heintz, R.A., Rice, S.D., 2004b. Relative potency of PAHs and heterocycles as aryl hydrocarbon receptor agonists in fish. Mar. Environ. Res. 58, 95–100.

Belair, C.D., Peterson, R.E., Heideman, W., 2001. Disruption of erythropoiesis by dioxin in the zebrafish. Dev. Dyn. 222, 581–594.

Cantrell, S.M., Joy-Schlezinger, J., Stegeman, J.J., Tillitt, D.E., Hannink, M., 1998. Correlation of 2,3,7,8-tetrachlorodibenzo-*p*-dioxin-induced apoptotic

cell death in the embryonic vasculature with embryotoxicity. Toxicol. Appl. Pharmacol. 148, 24–34.

Cantrell, S.M., Lutz, L.H., Tillitt, D.E., Hannink, M., 1996. Embryotoxicity of 2,3,7,8-tetrachlorodibenzo-*p*-dioxin (TCDD): the embryonic vasculature is a physiological target for TCDD-induced DNA damage and apoptotic cell death in medaka (*Orizias latipes*). Toxicol. Appl. Pharmacol. 141, 23–34.

Carls, M.G., Rice, S.D., Hose, J.E., 1999. Sensitivity of fish embryos to weathered crude oil: Part I. Low-level exposure during incubation causes malformations, genetic damage, and mortality in larval Pacific herring (*Clupea pallasi*). Environ. Toxicol. Chem. 18, 481–493.

Carney, S.A., Peterson, R.E., Heideman, W., 2004. 2,3,7,8-Tetrachlorodibenzo-*p*-dioxin activation of the aryl hydrocarbon receptor/aryl hydrocarbon receptor nuclear translocator pathway causes developmental toxicity through a CYP1A-independent mechanism in zebrafish. Mol. Pharmacol. 66, 512–521.

Colavecchia, M.V., Backus, S.M., Hodson, P.V., Parrott, J.L., 2004. Toxicity of oil sands to early life stages of fathead minnows (*Pimephales promelas*). Environ. Toxicol. Chem. 23, 1709–1718.

Couillard, C.M., 2002. A microscale test to measure petroleum oil toxicity to mummichog embryos. Environ. Toxicol. 17, 195–202.

Di Toro, D.M., McGrath, J.A., 2000. Technical basis for narcotic chemicals and polycyclic aromatic hydrocarbon criteria. II. Mixtures and sediments. Environ. Toxicol. Chem. 19, 1971–1982.

Di Toro, D.M., McGrath, J.A., Hansen, D.J., 2000. Technical basis for narcotic chemicals and polycyclic aromatic hydrocarbon criteria: I. Water and tissue. Environ. Toxicol. Chem. 19, 1951–1970.

Dong, W., Teraoka, H., Yamazaki, K., Tsukiyama, S., Imani, S., Imagawa, T., Stegeman, J.J., Peterson, R.E., Hiraga, T., 2002. 2,3,7,8-Tetrachlorodibenzo-*p*-dioxin toxicity in the zebrafish embryo: local circulation failure in the dorsal midbrain is associated with increased apoptosis. Toxicol. Sci. 69, 191–201.

French-McCay, D.P., 2002. Development and application of an oil toxicity and exposure model, OilToxEx. Environ. Toxicol. Chem. 21, 2080–2094.

French-McCay, D.P., 2004. Oil spill impact modeling: development and validation. Environ. Toxicol. Chem. 23, 2441–2456.

Fukunaga, B.N., Probst, M.R., Reisz-Porszasz, S., Hankinson, O., 1995. Identification of functional domains of the aryl hydrocarbon receptor. J. Biol. Chem. 270, 29270–29278.

Guiney, P.D., Smolowitz, R.M., Peterson, R.E., Stegeman, J.J., 1997. Correlation of 2,3,7,8-tetrachlorodibenzo-*p*-dioxin induction of cytochrome P4501A in vascular endothelium with toxicity in early life stages of lake trout. Toxicol. Appl. Pharmacol. 143, 256–273.

Guiney, P.D., Walker, M.K., Spitsbergen, J.M., Peterson, R.E., 2000. Hemodynamic dysfunction and cytochrome P4501A mRNA expression induced by 2,3,7,8-tetrachlorodibenzo-*p*-dioxin during embryonic stages of lake trout development. Toxicol. Appl. Pharmacol. 168, 1–14.

Hahn, M.E., 2002. Aryl hydrocarbon receptors: diversity and evolution. Chem. Biol. Interact. 141, 131–160.

Hahn, M.E., Karchner, S.I., 1995. Evolutionary conservation of the vertebrate Ah (dioxin) receptor: amplification and sequencing of the PAS domain of a teleost Ah receptor cDNA. Biochem. J. 310, 383–387.

Heintz, R.A., Short, J.W., Rice, S.D., 1999. Sensitivity of fish embryos to weathered crude oil: Part II. Increased mortality of pink salmon (*Oncorhynchus gorbuscha*) embryos incubating downstream from weathered Exxon Valdez crude oil. Environ. Toxicol. Chem. 18, 494–503.

Heintz, R.A., Rice, S.D., Wertheimer, A.C., Bradshaw, R.F., Thrower, F.P., Joyce, J.E., Short, J.W., 2000. Delayed effects on growth and marine survival of pink salmon *Oncorhynchus gorbuscha* after exposure to crude oil during embryonic development. Mar. Ecol. Prog. Ser. 208, 205–216.

Henry, T.R., Spitsbergen, J.M., Hornung, M.W., Abnet, C.C., Peterson, R.E., 1997. Early life stage toxicity of 2,3,7,8-tetrachlorodibenzo-*p*-dioxin in zebrafish (*Danio rerio*). Toxicol. Appl. Pharmacol. 142, 56–68.

Herrmann, C., Wray, J., Travers, F., Barman, T., 1992. Effect of 2,3-butanedione monoxime on myosin and myofibrillar ATPases. An example of an uncompetitive inhibitor. Biochemistry 31, 12227–12232.

Hestermann, E.V., Stegeman, J.J., Hahn, M.E., 2000. Relative contributions of affinity and intrinsic efficacy to aryl hydrocarbon receptor ligand potency. Toxicol. Appl. Pharmacol. 168, 160–172.

Hu, N., Sedmera, D., Yost, H.J., Clark, E.B., 2000. Structure and function of the developing zebrafish heart. Anat. Rec. 260, 148–157.

Incardona, J.P., Collier, T.K., Scholz, N.L., 2004. Defects in cardiac function precede morphological abnormalities in fish embryos exposed to polycyclic aromatic hydrocarbons. Toxicol. Appl. Pharmacol. 196, 191–205.

Incardona, J.P., Carls, M.G., Teraoka, H., Sloan, C.A., Collier, T.K., Scholz, N.L., 2005. Aryl hydrocarbon receptor-independent toxicity of weathered crude oil during fish development. Environ. Health Perspect. 113, 1755–1762.

Isogai, S., Lawson, N.D., Torrealday, S., Horiguchi, M., Weinstein, B.M., 2003. Angiogenic network formation in the developing vertebrate trunk. Development 130, 5281–5290.

Karchner, S.I., Franks, D.G., Hahn, M.E., 2005. AHR1B, a new functional aryl hydrocarbon receptor in zebrafish: tandem arrangement of *ahr1b* and *ahr2* genes. Biochem. J., vol. 392.

Karchner, S.I., Powell, W.H., Hahn, M.E., 1999. Identification and functional characterization of two highly divergent aryl hydrocarbon receptors (AHR1 and AHR2) in the teleost *Fundulus heteroclitus*. Evidence for a novel subfamily of ligand-binding basic helix loop helix-Per-ARNT-Sim (bHLH-PAS) factors. J. Biol. Chem. 274, 33814–33824.

Li, D., Daler, D., 2004. Ocean pollution from land-based sources: East China Sea, China. Ambio 33, 107–113.

Lima, A.L.C., Eglinton, T.I., Reddy, C.M., 2002. High-resolution record of pyrogenic polycyclic aromatic hydrocarbon deposition during the 20th century. Environ. Sci. Technol. 37, 53–61.

Linbo, T.L., Stehr, C.M., Incardona, J.P., Scholz, N.L., 2006. Dissolved copper triggers cell death in the peripheral mechanosensory system of larval fish. Environ. Toxicol. Chem. 25, 597–603.

Mackay, D., 1982. Correlation of bioconcentration factors. Environ. Sci. Technol. 16, 274–278.

Mackay, D., Puig, H., McCarty, L.S., 1992a. An equation describing the time course and variability in uptake and toxicity of narcotic chemicals to fish. Environ. Toxicol. Chem. 11, 941–951.

Mackay, D., Shiu, W.Y., Ma, K.C., 1992b. Illustrated Handbook of Physical–Chemical Properties and Environmental Fate for Organic Chemicals. Lewis Publishers, Boca Raton, FL.

Marty, G.D., Short, J.W., Dambach, D.M., Willits, N.H., Heintz, R.A., Rice, S.D., Stegeman, J.J., Hinton, D.E., 1997. Ascites, premature emergence, increased gonadal cell apoptosis, and cytochrome P4501A induction in pink salmon larvae continuously exposed to oil-contaminated gravel during development. Can. J. Zool.-Rev. Can. Zool. 75, 989–1007.

McCarty, L.S., Mackay, D., Smith, A.D., Ozburn, G.W., Dixon, D.G., 1992. Residue-based interpretation of toxicity and bioconcentration qsars from aquatic bioassays—Neutral narcotic organics. Environ. Toxicol. Chem. 11, 917–930.

Milan, D.J., Giokas, A.C., Serluca, F.C., Peterson, R.T., Macrae, C.A., 2006. Notch1b and neuregulin are required for specification of central cardiac conduction tissue. Development 133, 1125–1132.

Myers, C.R., Sutherland, L.A., Haasch, M.L., Lech, J.J., 1993. Antibodies to a synthetic peptide that react specifically with rainbow-trout hepatic cytochrome-P450 1a1. Environ. Toxicol. Chem. 12, 1619–1626.

National Research Council, 2003. Oil in the Sea III: Inputs, Fates, and Effects. National Academies Press, Washington, DC, p. 446.

Nebert, D.W., Dalton, T.P., Okey, A.B., Gonzalez, F.J., 2004. Role of aryl hydrocarbon receptor-mediated induction of the CYP1 enzymes in environmental toxicity and cancer. J. Biol. Chem. 279, 23847–23850.

Park, S.S., Miller, H., Klotz, A.V., Kloepper-Sams, P.J., Stegeman, J.J., Gelboin, H.V., 1986. Monoclonal antibodies to liver microsomal cytochrome P-450E of the marine fish *Stenotomus chrysops* (scup): cross reactivity with 3-methylcholanthrene induced rat cytochrome P-450. Arch. Biochem. Biophys. 249, 339–350.

Partridge, V., Welch, K., Aasen, S., Dutch, M., 2005. Temporal monitoring of Puget Sound sediments: Results of the Puget Sound Ambient Monitoring Program, 1989–2000. Washington State Department of Ecology, Olympia (05-03-016, 267 pp.).

Peterson, R.E., Theobald, H.M., Kimmel, G.L., 1993. Developmental and reproductive toxicity of dioxins and related compounds: cross-species comparisons. Crit. Rev. Toxicol. 23, 283–335.

Pollino, C.A., Holdway, D.A., 2002. Toxicity testing of crude oil and related compounds using early life stages of the crimson-spotted rainbowfish (*Melanotaenia fluviatilis*). Ecotox. Environ. Safe 52, 180–189.

Prasch, A.L., Teraoka, H., Carney, S.A., Dong, W., Hiraga, T., Stegeman, J.J., Heideman, W., Peterson, R.E., 2003. Aryl hydrocarbon receptor 2 mediates 2,3,7,8-tetrachlorodibenzo-*p*-dioxin developmental toxicity in zebrafish. Toxicol. Sci. 76, 138–150.

Rombough, P., 2002. Gills are needed for ionoregulation before they are needed for O(2) uptake in developing zebrafish, *Danio rerio*. J. Exp. Biol. 205, 1787–1794.

Rottbauer, W., Baker, K., Wo, Z.G., Mohideen, M.A., Cantiello, H.F., Fishman, M. C., 2001. Growth and function of the embryonic heart depend upon the cardiac-specific L-type calcium channel alpha1 subunit. Dev. Cell 1, 265–275.

Roy, N.K., Wirgin, I., 1997. Characterization of the aromatic hydrocarbon receptor gene and its expression in Atlantic tomcod. Arch. Biochem. Biophys. 344, 373–386.

Safe, S., 1990. Polychlorinated biphenyls (PCBs), dibenzo-*p*-dioxins (PCDDs), dibenzofurans (PCDFs), and related compounds: environmental and mechanistic considerations which support the development of toxic equivalency factors (TEFs). Crit. Rev. Toxicol. 21, 51–88.

Schmidt, J.V., Bradfield, C.A., 1996. Ah receptor signaling pathways. Annu. Rev. Cell Dev. Biol. 12, 55–89.

Sehnert, A.J., Huq, A., Weinstein, B.M., Walker, C., Fishman, M., Stainier, D.Y., 2002. Cardiac troponin T is essential in sarcomere assembly and cardiac contractility. Nat. Genet. 31, 106–110.

Serluca, F.C., Drummond, I.A., Fishman, M.C., 2002. Endothelial signaling in kidney morphogenesis: a role for hemodynamic forces. Curr. Biol. 12, 492–497.

Sundberg, H., Ishaq, R., Akerman, G., Tjarnlund, U., Zebuhr, Y., Linderoth, M., Broman, D., Balk, L., 2005. A bio-effect directed fractionation study for toxicological and chemical characterization of organic compounds in bottom sediment. Toxicol. Sci. 84, 63–72.

Tanguay, R.L., Abnet, C.C., Heideman, W., Peterson, R.E., 1999. Cloning and characterization of the zebrafish (*Danio rerio*) aryl hydrocarbon receptor. Biochim. Biophys. Acta 1444, 35–48.

Teraoka, H., Dong, W., Tsujimoto, Y., Iwasa, H., Endoh, D., Ueno, N., Stegeman, J.J., Peterson, R.E., Hiraga, T., 2003. Induction of cytochrome P450 1A is required for circulation failure and edema by 2,3,7,8-tetrachlorodibenzo-*p*-dioxin in zebrafish. Biochem. Biophys. Res. Commun. 304, 223–228.

Trant, J.M., Gavasso, S., Ackers, J., Chung, B.C., Place, A.R., 2001. Developmental expression of cytochrome P450 aromatase genes (CYP19a and CYP19b) in zebrafish fry (*Danio rerio*). J. Exp. Zool. 290, 475–483.

U.S. EPA, 2003. Procedures for the derivation of equilibrium partitioning sediment benchmarks (ESBs) for the protection of benthic organisms: PAH mixtures. EPA Office of Research and Development, Washington, DC. (EPA-600-R-02-013).

Van Metre, P.C., Mahler, B.J., 2003. The contribution of particles washed from rooftops to contaminant loading to urban streams. Chemosphere 52, 1727–1741.

Van Metre, P.C., Mahler, B.J., Furlong, E.T., 2000. Urban sprawl leaves its PAH signature. Environ. Sci. Technol. 34, 4064–4070.

Vines, C.A., Robbins, T., Griffin, F.J., Cherr, G.N., 2000. The effects of diffusible creosote-derived compounds on development in Pacific herring (*Clupea pallasi*). Aquat. Toxicol. 51, 225–239.